Phase diagram studies on iron and nickel silicides: high-pressure experiments and *ab initio* calculations

To cite this article: D Santamaría-Perez *et al* 2008 *J. Phys.: Conf. Ser.* **121** 022013

View the article online for updates and enhancements.

Related content

- Reflection electron energy loss spectroscopy of structures based on silicon and transition metals
A S Parshin, A Yu Igumenov, Yu L Mikhlin et al.

- Opportunities of research in multiferroic materials using Angle Dispersive X-ray Diffraction (ADXRD) beamline on Indus-2 synchrotron source
A K Sinha, M N Singh, A Upadhyay et al.

- A High-Pressure Apparatus for TOF Neutron Diffraction
Kazuo Kamigaki

Phase diagram studies on iron and nickel silicides: High-pressure experiments and *ab initio* calculations

D. Santamaría-Perez[1,2]**, D. Errandonea**[3,*]**, A. Vegas**[2]**, J. Nuss**[4]**, M. Jansen**[4]**, P. Rodríguez-Hernández**[5]**, A. Muñoz**[5]**, and R. Boehler**[1]

[1]Max-Planck Institut für Chemie, Postfach 3060, D-55020 Mainz, Germany

[2]Instituto de Química-Física Rocasolano, CSIC, C/Serrano 119, 28006 Madrid, Spain

[3]MALTA Consolider Team, Departamento de Física Aplicada-ICMUV, Univiversitat de València, C/Dr.Moliner 50, 46100 Burjassot, Spain

[4]MPI für Festkörperforschung, Heisenbergstrasse 1, 70569 Stuttgart, Germany

[5]MALTA Consolider Team, Departamento de Física Fundamental II, Universidad de La Laguna, La Laguna, Tenerife, Spain

Email: daniel.errandonea@uv.es

Abstract. We performed high-pressure ADXRD studies on Fe_5Si_3 and Ni_2Si up to 75 GPa. No evidence of the occurrence of a phase transition was observed in them. Fe_5Si_3 was found to compress isotropically, but an anisotropic compression was observed in Ni_2Si. These results are supported by *ab initio* total-energy calculations, which for Fe_5Si_3 also predicted a transition at 283 GPa from the hexagonal *P6₃/mcm* phase to a cubic phase. High-pressure melting studies were conducted on FeSi up to 70 GPa. We found a change in the melting slope at 12 GPa, which is attributed to the intersection of the melting curve with the phase boundary between ε-FeSi and CsCl-type FeSi. Finally, an equation of state for Fe_5Si_3 and Ni_2Si is reported.

1. Introduction

Iron silicides are probable candidates of the origin of the ultra-low velocity zone at the base of the Earth's mantle. They may appear at the core-mantle boundary since liquid iron coexists with solid silicates. In addition, the high P-T phase diagram of FeSi is currently of interest since silicon is a possible major alloying element in the Earth's outer core. In order to address these issues, several studies on iron silicides under pressure have been done [1–3]. On the other hand, iron and nickel silicides have received attention since their magnetic and electronic properties make them prospective materials for optoelectronics [4]. Finally, these silicides also produce oxides in which the Fe:Si (Ni:Si) stoichiometry is maintained. For example, Fe_5Si_3 (the mineral xifengite) produces the garnet $Fe_5Si_3O_{12}$ whose Fe_5Si_3 subarray differs from the crystal structure of the alloy itself. As in some cases, the cation subarray of the oxide reproduces the structure of the high-pressure phase of the precursor alloy [5], it has been predicted that at high pressure the Fe_5Si_3 alloy would undergo a phase transition to a structure, which may reproduce that of the cation array in $Fe_5Si_3O_{12}$. Because of these reasons, iron and nickel silicides are interesting compounds from geophysical, technological, and crystallochemichal points of view.

---

[*] To whom any correspondence should be addressed.

Here we present new studies of the high P-T phase-diagram of iron and nickel silicides. Angle dispersive x-ray diffraction (ADXRD) experiments were performed on Fe_5Si_3 and Ni_2Si up to 75 GPa. High-pressure melting studies were carried out in FeSi up to 70 GPa. We found that Fe_5Si_3 remains stable in the hexagonal $P6_3/mcm$ phase (SG No. 193) up to the highest pressure reached in our experiments and Ni_2Si remains stable in the orthorhombic *Pbnm* structure (SG No. 62). We also found at 12 GPa a change in the slope of the melting curve of FeSi, which agrees with the occurrence of the phase transition between ε-FeSi and CsCl-type FeSi. The experimental results were supported by *ab initio* total-energy calculations. The calculations also predict the presence beyond 283 GPa of a new denser phase in Fe_5Si_3, which has the structure adopted by Fe and Si in $Fe_5Si_3O_{12}$. Finally, an equation of state (EOS) for Fe_5Si_3 and Ni_2Si was obtained. The reported results could have important implications for the differentiation processes of the planets and the composition of their cores.

2. Experimental details

Fe_5Si_3 and Ni_2Si were synthesized by solid state reaction from stoichiometric amounts of high-purity elements. Samples were prepared as finely ground powders from these materials. High-pressure ADXRD measurements were carried out in a 300-μm culet Mao-Bell DAC. The samples were loaded into a 100-μm-diameter hole drilled on a rhenium gasket. Silicone oil was used as pressure-transmitting medium. Pressure was determined using the ruby fluorescence method [6]. The ADXRD studies were performed at the 16-IDB beamline of the HPCAT at the Advanced Photon Source (APS). The x-ray beam ($λ = 0.3931$ Å) was focused down to 10 x 10 $μm^2$. Diffraction images were recorded with a Mar345 image-plate detector and were integrated and corrected for distortions using FIT2D. Indexing, structure solution, and refinements were performed using DICVOL and POWDERCELL.

In the melting experiments high-purity FeSi samples (Alpha Aesar) were compressed in a DAC equipped with 300-μm culet anvils with conical supports [7]. Samples were around 40 μm in diameter and 10 μm thick. The sample chamber was a 100-μm-diameter hole drilled in tungsten gasket. High-purity KBr, KCl, and CsCl were used as pressure media and to thermally isolate the samples from the diamonds [8, 9]. FeSi was heated at high pressure with a Nd:YVO$_4$ infrared laser (TEM$_{00}$ mode, $λ = 1.064$ μm). Melting was detected by the laser-speckle method [10-12]. Each data point reported is the average of five experiments. Temperatures were determined by fitting a Planck function to the thermal emission spectra of the sample [9, 13] measured in the 500-900 nm spectral range. Pressure was measured before and after heating using the ruby fluorescence method [6]. During the experiments, the heated sample is subjected to a pressure relaxation, due to annealing of the pressure medium, and to a thermal pressure increase. Uncertainty in pressure is about 1 GPa [8, 14]. After each experiment, the samples were recovered and inspected, not showing signs of reaction or oxidation.

3. Overview of the calculations

The structural stability of the phases of Fe_5Si_3 and Ni_2Si was further investigated theoretically by means of total-energy calculations performed within the framework of DFT with the Vienna *ab initio* simulation package (VASP) [15]. A review of DFT-based total-energy methods as applied to the study of phase stability can be found in Ref. [16]. The exchange and correlation energy was described within the generalized gradient approximation [17]. We used ultrasoft pseudopotentials and we adopted the projector augmented wave scheme. We employed a basis set of plane waves up to a kinetic energy cutoff of 334.9 eV for Fe_5Si_3 and 336.9 eV for Ni_2Si, and Monkhorts-Pack grids for the Brillouin-zone integrations which ensure highly converged results (to about 1 meV per formula unit). At each selected volume for a given structure the external and internal parameters are relaxed through the calculations of the forces on the atoms and the components of the stress tensor. Valuable structural information for each phase was obtained from the calculated energy-volume curves after an EOS fitting.

4. Results and discussion

4.1 Structural studies of Fe_5Si_3

Fig. 1 shows our ADXRD data for Fe_5Si_3 at selected pressures and compares them with a diffraction pattern measured at atmospheric pressure (0.0001 GPa) outside the DAC. This pattern corresponded to the hexagonal *P6₃/mcm* structure, with no indication of any additional phase in it. The unit-cell parameters were a = 6.752(5) Å and c = 4.740(3) Å, in agreement with Ref. [3]. Under compression, the only changes we observed in the x-ray diffraction patterns are the typical peak broadening of DAC experiments [18, 19] and the appearance of a peak around 2θ = 11°. This peak has been assigned to a gasket line and can be easily identified since its pressure shift is smaller than that of the Fe_5Si_3 peaks. Regarding the Fe_5Si_3 peaks, we observed that they shift smoothly with compression and that all the Bragg reflections present in the diffraction patterns can be indexed with the *P6₃/mcm* structure up to 75 GPa. From the diffraction data, we obtained the evolution with pressure of the volume and lattice parameters of Fe_5Si_3. These results are shown in Fig. 2, where we compare them with previous data obtained using NaCl as pressure medium [3]. Both experiments agree within their accuracy up to 20 GPa. Above this pressure, the former study slightly underestimates the decrease of the volume. This fact can be due to the larger non-hydrostatic stresses caused by the NaCl pressure medium [20, 21].
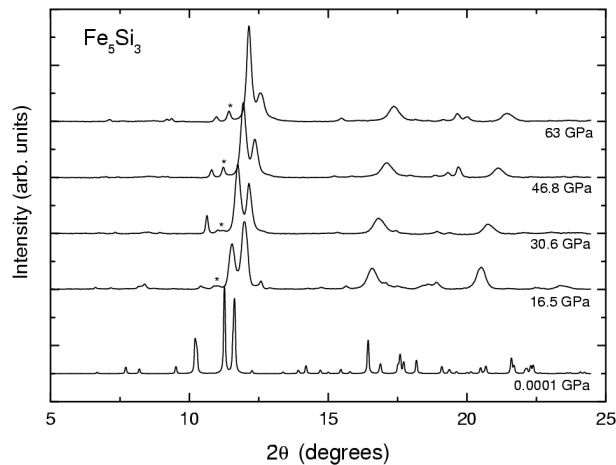

Figure 1: Room-temperature ADXRD data of Fe_5Si_3 at different pressures. In all diagrams the background was subtracted. The gasket peak is denoted by the symbol *. Pressures are indicated in the figure.

Our pressure-volume data shown in Fig. 2 have been fitted using a third-order Birch-Murnaghan EOS [22]. By fixing V_0 = 187.154 Å^3 we obtained B_0 = 215 ± 14 GPa and B_0' = 3.6 ± 0.6. The bulk modulus obtained from our data is slightly smaller than that reported in Ref. [3], but their difference is smaller than those found for other iron silicides [2, 23 – 25]. In our case, the differences in B_0 may be caused by two facts: 1) The data reported in Ref. [3] gives a smaller compressibility than the present data for P ≥ 20 GPa. 2) A Murnaghan EOS [26] was used in Ref. [3] to fit B_0 and B_0' overestimating the bulk modulus. Let us mention here that the B_0 of Fe_5Si_3 is larger than the B_0 of ε-FeSi (B_0 = 160 - 200 GPa) [2, 23, 24], CsCl-type FeSi (B_0 = 184 GPa) [27], α-FeSi$_2$ (B_0 = 182 GPa) [28], β-FeSi$_2$ (B_0 = 180 - 200 GPa) [25], and Fe_7Si_3 (B_0 = 199 -207 GPa) [2, 29]. The compressibility of iron silicides has been proposed to be correlated with the coordination number (CN) of the minority element [3]. In Fe_5Si_3 the silicon atoms have a CN = 9, whereas in the other alloys 6 ≤ CN ≤ 8. This fact makes Fe_5Si_3 the least compressible compound among the different iron silicides studied up to now.

Fig. 2 shows that the compression of Fe_5Si_3 is isotropic. The same fact was observed in Ref. [3] up to 30 GPa. Our experiments verify that the compression of Fe_5Si_3 remains isotropic up to 75 GPa. A quadratic fit to our data gives the following pressure dependence of the unit-cell parameters of Fe_5Si_3:

$$a = 6.76(1) - 9.5(6)\ 10^{-3}\ P + 3.5(7)\ 10^{-5}\ P^2 \qquad \text{and}$$

$$c = 4.736(9) - 7.5(5)\ 10^{-3}\ P + 3.8(6)\ 10^{-5}\ P^2,$$

where *a* and *c* are given in Å and P is given in GPa. From these two relations it can be estimated that from 0.0001 GPa to 75 GPa *a* and *c* are reduced approximately a 7.5%.

We compare now our experimental and theoretical results. Fig. 3 shows the energy-volume curves for the different structures considered for Fe_5Si_3, from which the relative stability of the different phases can be extracted. This figure shows the hexagonal *P6₃/mcm* structure to be stable up to 283 GPa, which agrees with the absence of phase transitions observed in the experiments. At ambient pressure we obtained for the *P6₃/mcm* structure $V_0 = 175.7$ Å^3, $B_0 = 238.76$ GPa and $B_0' = 3.8$. These values compares well with the experimental results, with differences within the typical systematic errors in DFT calculations. A similar degree of agreement exists for the calculated internal parameters $x_1 = 0.2450$ for the Fe 6g atoms, and $x_2 = 0.6044$ for the Si 6g atoms (experimental: 0.2307 and 0.597, respectively) and *c/a* ratio = 0.719. Our calculations also confirm that the compression of Fe_5Si_3 is isotropic up to 283 GPa; i.e. in the whole range of stability of the hexagonal phase of Fe_5Si_3. As pressure increases, the *P6₃/mcm* structure becomes unstable and converts to a body center cubic phase (SG $Ia\overline{3}d$, No. 230) with Fe atoms in 24c and 16a positions, and the Si atoms in 24d positions. This phase is isomorphous to the structure adopted by the Fe_5Si_3 subarray in the $Fe_5Si_3O_{12}$ garnet. This fact is in good agreement with the hypothesis that proposes the existence of a correlation between oxidation and pressure [5]. The high-pressure phase only emerges as thermodynamically stable above a compression threshold of 283 GPa. From the common tangent construction or the enthalpy versus pressure plot, our calculations predict that Fe_5Si_3 becomes unstable in the *P6₃/mcm* phase at 283 GPa against the cubic $Ia\overline{3}d$ phase. The transition is of first-order with a volume change of 1.1 %. The EOS fitting gives $V_0 = 346.60$, $B_0 = 249.95$ GPa and $B_0' = 3.77$ for the predicted high-pressure phase.
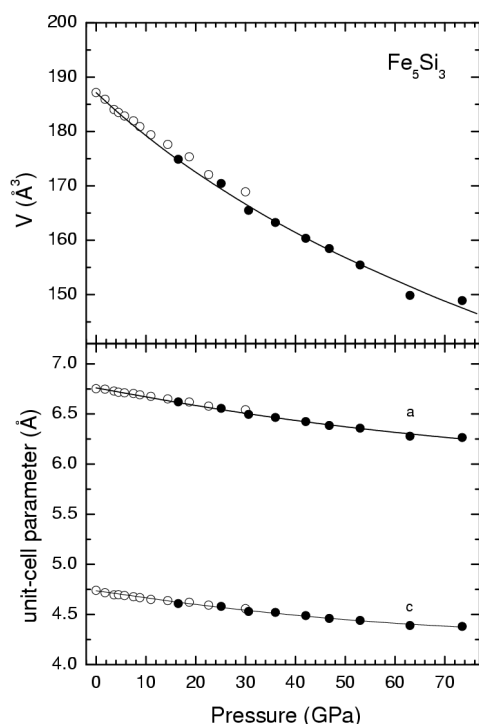

Figure 2: Volume and lattice parameters of Fe_5Si_3 under pressure. Solid circles: present data. Empty circles: data of Ref. [3]. Solid lines: fitted EOS and quadratic fits to *a* and *c*.
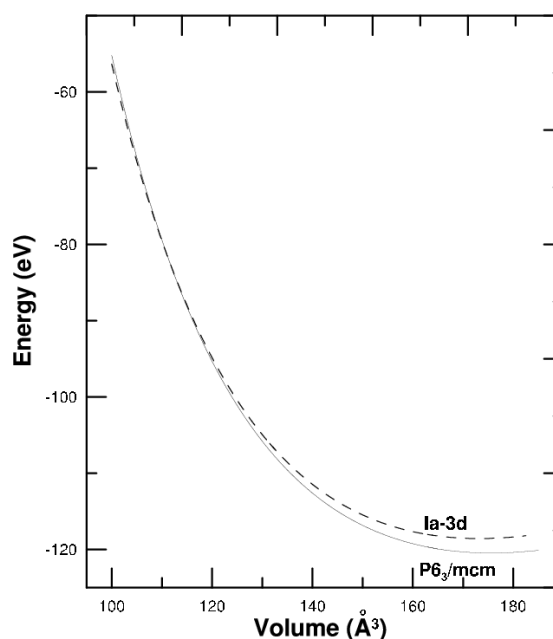
Figure 3: Total-energy versus volume from *ab initio* calculations for the analysed structures of Fe_5Si_3. (Volume and energy are per two formula units).

4.2 Structural studies of Ni_2Si

At atmospheric pressure, the diffraction pattern for Ni_2Si corresponded to the *Pbnm* structure, with no indication of any extra phase in it. The unit-cell parameters were $a = 7.059(7)$ Å, $b = 4.990(5)$ Å, and $c = 3.719(4)$ Å, in agreement with Ref. [30]. Upon compression, we observed that the Ni_2Si peaks shift smoothly and that all of them can be assigned to the *Pbnm* structure up to 75 GPa. From our diffraction data, we obtained the pressure evolution of the volume and lattice parameters of Ni_2Si. These results are plotted in Fig. 4. They have been analysed using a third-order Birch-Murnaghan EOS [22]. By fixing $V_0 = 131.049$ Å^3 we obtained $B_0 = 147 \pm 5$ GPa and $B_0' = 4.5 \pm 0.5$.

Fig. 4 shows that the compression Ni_2Si of is highly anisotropic. In particular the *c*-axis is much less compressible that the other two crystalline axis. A quadratic fit to our data gives the following pressure dependence for the unit-cell parameters of Ni_2Si:

$$a = 7.00(5) - 2.6(6)\ 10^{-2}\ P + 2.0(3)\ 10^{-4}\ P^2\ ,$$

$$b = 5.085(9) - 1.0(3)\ 10^{-2}\ P + 4(1)\ 10^{-5}\ P^2\ , \qquad \text{and}$$

$$c = 3.278(6) - 2.4(4)\ 10^{-3}\ P + 3.6(9)\ 10^{-6}\ P^2,$$

where *a*, *b*, and *c* are given in Å and P is given in GPa. From these three relations it can be estimated that from 0.0001 GPa to 75 GPa *a* is reduced a 12.7%, *b* is reduced a 9.3%, and *c* is reduced a 3.9%. The last result implies that the linear incompressibility of Ni_2Si along the *c*-axis is similar to that of diamond. The structure of Ni_2Si can be described in terms of columns of face-sharing Ni_6Si trigonal prisms connected by edge-sharing to form layers perpendicular to the *a*-axis. As observed in other crystals [31], a consequence of this layered structure is the anisotropic compressibility of Ni_2Si.
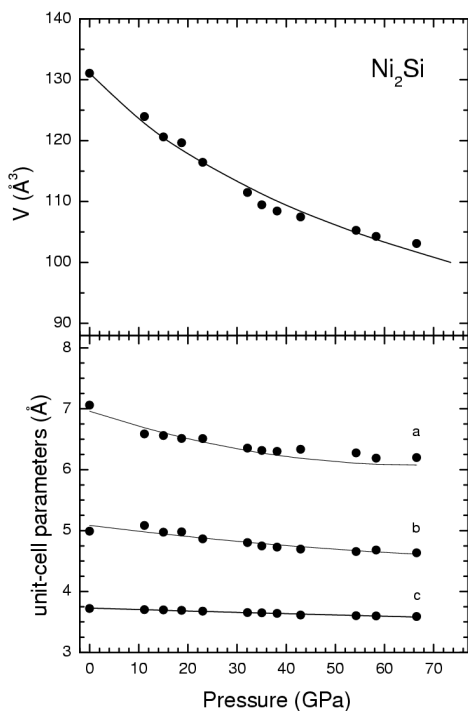

Figure 4: Volume and lattice parameters of Ni_2Si under pressure. Solid circles: present data. Solid lines: fitted EOS and quadratic fits to *a*, *b*, and *c*.
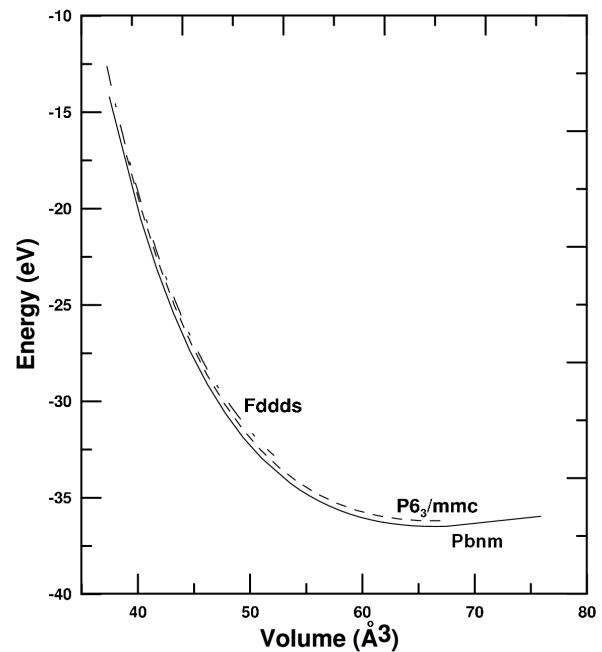
Figure 5: Total-energy versus volume from *ab initio* calculations for the analysed structures of Ni_2Si. (Volume and energy are per two formula units).

We compare now our experimental data with the results from our calculations. Fig. 5 shows the energy-volume curves for the different structures considered for Ni_2Si, from which the relative

stability of the different phases can be extracted. We select some candidate structures, the *Fddds* structure (SG No. 70) and the *P6₃/mmc* structure (SG No. 194) adopted by other A_2X compounds like Si_2Ti and Ni_2In. Fig. 5 shows the orthorhombic *Pbnm* structure to be stable up to nearly 400 GPa, which agrees with the absence of phase transitions observed in the experiments. Our calculations also confirm that the compression of Ni_2Si is highly anisotropic. They also give for the *Pbnm* structure the following EOS parameters: $V_0 = 133.44$ Å^3, $B_0 = 175.07$ GPa and $B_0' = 5$. The calculated values of the internal parameters agree very well with the experimental values $x_1 = 0.0606$, $y_1 = 0.3304$, $x_2 = 0.2039$, $y_2 = 0.0404$ for the Ni 4c atoms, and $x_3 = 0.3855$, $y_3 = 0.2862$ for the Si 4c atoms.

4.3 Melting studies of FeSi

Fig. 6 shows the melting curve of iron silicide. The data obtained using different pressure media are consistent among themselves, indicating that the observed melting temperatures are independent of the pressure medium employed. Initially, the melting curve is flat, with a melting temperature close to 1700 K. However, at 12 GPa, we found that a change in the slope of the melting curve of FeSi takes place. The melting slope beyond 12 GPa is 40 K/GPa, but the melting curve of FeSi considerable flattens at high pressures as occurs in many metals [11]. The melting slope at 70 GPa is 10 K/GPa. The observed change in the melting slope at 12 GPa indicates the presence of a triple point, which can be assigned to the intersection of the phase boundary between the ε-phase and CsCl-phase of FeSi [1] with the melting line (see Fig. 6). The melting slope can be calculated using the Clausius–Clapeyron equation $dT/dP = \Delta V/\Delta S$, where ΔV and ΔS are, respectively, the difference in molar volume and entropy of the solid and liquid coexisting phases. According to this equation, it is reasonable to expect that the volume difference between the two solid phases of FeSi [1] would produce a discontinuous change of melting slope at the solid-solid-liquid triple point [32, 33]. Finally, it is important to note that the melting curve for FeSi crosses the melting curve of iron at 32 GPa and 2400 K [14].
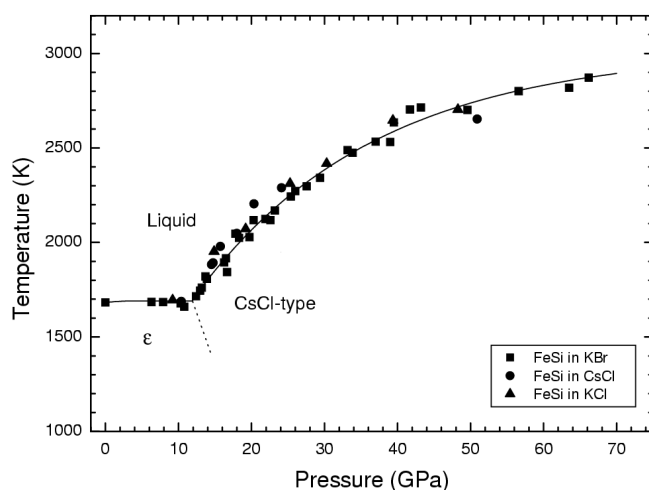

Figure 6: Melting curve of FeSi. Our melting data are represented by solid symbols. The different pressure media used in the experiments are indicated in the inset. The solid line is a fit to the experimental data. The dotted line schematically represents the phase boundary between ε-FeSi and CsCl-type FeSi.

5. Concluding Remarks

The high P-T phase diagrams of iron and nickel silicides have been studied by means of x-ray diffraction and melting experiments as well as by *ab initio* calculations. In the experiments we observed the absence of phase transitions in Fe_5Si_3 and Ni_2Si up to 75 GPa. We also found that the compression of Fe_5Si_3 is rather isotropic whereas the compression of Ni_2Si is highly anisotropic. The experimental results are supported by the total-energy calculations, which also predict the occurrence of a phase transition in Fe_5Si_3 at 283 GPa from the hexagonal *P6₃/mcm* phase to a cubic phase belonging to space group $Ia\bar{3}d$. On the other hand, the calculations predict that the *Pbnm* structure of Ni_2Si is the most stable structure at least up to 400 GPa. In the melting experiments, the melting curve of FeSi was determined up to 70 GPa showing a change in the melting slope at 12 GPa, likely due to

the first-order phase transition between ε-FeSi and the CsCl-type FeSi structures. Finally an EOS was determined for Fe_5Si_3 (Ni_2Si) giving the following parameters: V_0 = 187.154 Å^3, B_0 = 215 ± 14 GPa, and B_0' = 3.6 ± 0.6 (V_0 = 131.049 Å^3, B_0 = 147 ± 5 GPa, and B_0' = 4.5 ± 0.5).

References
[1] D.P. Dobson, L. Vocadlo, and I.G. Wood, 2002 *Am. Mineral.* **87** 784.
[2] J.F. Lin, A. J. Campbell, D.L. Heinz, and G.Y. Shen, 2003 *J. Geophysical Research* **108** 2045.
[3] D. Santamaria-Perez, J. Nuss, J. Haines, M. Jansen, and A. Vegas, 2004 *Solid State Sciences* **6** 673.
[4] K. Takarabe, T. Suemasu, Y. Ikura, and F. Hasegawa, 2002 *J. Appl. Phys. Jpn.* **39** L789.
[5] A. Vegas and M. Jansen, 2002 *Acta Cryst. B* **58** 38.
[6] H. K. Mao, J. Xu, and P. M. Bell, 1986 J. *Geophys. Res.* **91** 4673.
[7] R. Boehler and K. De Hantsetters, 2004 *High Pres. Res.* **24** 391.
[8] R. Boehler, 2000 *Rev. Geophys.* **38** 221.
[9] D. Errandonea, 2006 *J. Phys. Chem. Solids* **67** 2017.
[10] R. Boehler, 1993 *Nature* **363** 534.
[11] D. Errandonea, B. Schwager, R. Ditz, C. Gessmann, R. Boehler, and M. Ross, 2003 *Phys. Rev. B* **63** 132104.
[12] D. Errandonea, M. Somayazulu, D. Häusermann, and H.K. Mao, 2003 *J. Phys. Condens. Matter* **15** 7635.
[13] R. Boehler, 1986 *Geophys. Res. Lett.* **13** 1153.
[14] D. Errandonea, R. Boehler, B. Schwager, and M. Mezouar, 2007 *Phys. Rev. B* **75** 014103.
[15] G. Kresse and J. Furthmüller, 1996 *Comput. Mater. Sci.* **6** 15; 1996 *Phys. Rev. B* **54** 11169.
[16] A. Mujica, A. Rubio, A. Muñoz, and R. J. Needs, 2003 *Rev. Mod. Phys.* **75** 863.
[17] J. P. Perdew, K. Burke and M. Ernzerhof, 1996 *Phys. Rev. Lett.* **77** 3865.
[18] D. He and T. Duffy, 2006 *Phys. Rev. B* **73** 134106.
[19] D. Errandonea, R. Boehler, S. Japel, M. Mezouar, and L. R. Benedetti, 2006 *Phys. Rev. B* **73** 092106.
[20] D. Errandonea, Y. Meng, M. Somayazulu, and D. Häusermann, 2005 *Physica B* **355** 116.
[21] D. Errandonea, J. Pellicer-Porres, F. J. Manjón, A. Segura, Ch. Ferrer-Roca, R. S. Kumar, O. Tschauner, P. Rodriguez-Hernandez, S. Radescu, J. Lopez-Solano, A. Mujica, A. Muñoz, and G. Aquilanti, 2005 *Phys. Rev. B* **72** 174106.
[22] F. Birch, 1978 *J. Geophys. Res.* **83** 1257.
[23] I.G. Wood, W.I.F. David, S. Hull, and G.D. Price, 1996 *J. Appl. Crystallogr.* **29** 215.
[24] L. Vocadlo, G.D. Price, and I.G: Wood, 2000 *Acta Crystal. B* **56** 369.
[25] K. Takarabe, R. Teranishi, J. Oinuma, and Y. Mori, 2002 *J. Phys. Condens. Matter* **14** 11007.
[26] F.D. Murnaghan, 1949 *Proc. Nat. Acad. Sciences* **30** 244.
[27] D.P. Dobson, W.A. Crichton, P. Bouvier, L. Vocadlo, and I.G. Wood, 2003 *Geophys. Res. Letters* **30** 1014.
[28] K. Takarabe, T. Ikai, Y. Mori, H. Udono, and I. Kikuma, 2004 *J. Appl. Phys.* **96** 4903.
[29] N. Hirao, E. Ohtani, T. Kondo, and T. Kikegawa., 2004 *Phys Chem. Minerals* **31** 329.
[30] K. Toman, 1952 *Acta Crystal.* **5** 329.

[31] D. Errandonea, D. Martínez-García, A. Segura, A. Chevy, G. Tobias, E. Canadell, and P. Ordejón, 2006 *Phys. Rev. B* **73** 235202.

[32] R. Boehler, D. Errandonea, M. Ross, 2002 *High Pressure Res.* **22** 479.

[33] D. Errandonea, 2005 *Physica B* **357** 356.